European Rotorcraft Forum

High-fidelity CFD Simulation and Optimisation of Ducted Propellers

Tao Zhang [1], George N. Barakos [2]
CFD Laboratory, School of Engineering, University of Glasgow

Abstract

This paper presents numerical analyses and optimisation of aerodynamics of ducted/un-ducted propellers, based on high-fidelity CFD methods with adjoint formulations. A ducted propeller test case by NASA is chosen as the validation case and baseline design. High-fidelity CFD simulations are performed using the in-house solver HMB3. An adjoint-based aerodynamic optimisation framework is proposed and applied to studies of the separate and coupled duct shape and blade twist designs for the ducted propeller, with blades resolved. A new parametrisation method for the duct shape is proposed, allowing variations in curve shapes and leading/trailing edge point positions. Sensitivities of the performance with respect to design variables of the duct shape and blade twist are solved using the HMB3 adjoint solver and are analysed in detail. Performance comparisons of the optimised designs are presented and detailed.

1 Introduction

The ducted propeller is a propeller enclosed by an annular duct. It has been widely used in marine propulsions [1], either to augment the thrust or to reduce tip speeds to alleviate cavitation. Applications in ducted wind turbines [2], albeit at small scale, are also popular. In very recent years, due to the emerging popularity of eVOTL vehicles, the ducted propeller is seen as a promising choice for propulsion and lift. The presence of the duct alters the mass and momentum flow rates through the rotor disk, thereby increasing or decreasing the propulsor thrust, depending on the specific duct shape. By shielding the propeller, the duct provides protection to ground personnel and equipment. In emergencies, the duct can contain the debris to prevent further damages to the airframe. Acoustic reduction is also expected due to the duct shielding [3]. A detailed review of ducted propeller research, in terms of experiments, numerical simulations and optimisation, and research challenges, is presented in Reference [4].

Many early tests [5] [6] [3] confirmed the superior efficiency of the ducted propeller over its un-ducted counter-part, in hover or at low advance ratios. It was observed that while higher mass flow rate is induced, the propeller works at higher axial inflow and is hence off-loaded, and the thrust augmentation is gained from the duct surface harvesting the pressure field. In hover, it is possible that the ducted propeller provides twice as much the thrust while producing almost the same torque as the open propeller equivalent, with the duct carrying about 60% of the total thrust [7]. However, as the advance ratio increases, the ducted propeller typically becomes inefficient and the duct contribution turns to drag. Overall, it can be seen that the duct shape plays a significant role in altering the total thrust and efficiency. It is therefore of interest to explore the sensitivity of the performance with respect to duct geometries, and to study if the high efficiency of the ducted propeller can be maintained at high advance ratios by modifying the duct geometry. In this respect, the gradient-based optimisation, combined with high-fidelity CFD methods, is especially suitable.

This works presents the high-fidelity CFD simulation and adjoint-based optimisation of ducted propellers in axial flight. Simulations of a ducted propeller test case by NASA [7] are performed, and the results are in good agreement with the experimental data. Parametrisation methods for the duct shape and the blade pitch distribution are proposed. A gradient-based optimisation framework is proposed and applied to the optimisation of the duct shape and the blade twist. The flow sensitivities are solved using the adjoint formulation implemented in HMB3. Changes in duct shapes and blade twist effectively increased the total thrust while maintaining the

[1] PhD Student - t.zhang.4@research.gla.ac.uk
[2] Professor - george.barakos@glasgow.ac.uk

similar level of efficiency. With duct shape and blade twist considered altogether in the coupled optimisation, large increases in thrust is achieved.

2 Numerical Methods

2.1 HMB3 Adjoint Solver

The Helicopter Multi-Block (HMB3) [8, 9, 10] code is used in the present work. The code has been widely used in simulations of rotorcraft flows [11, 12, 13, 14]. HMB3 solves the Unsteady Reynolds Averaged NavierStokes (URANS) equations in integral form using the Arbitrary Lagrangian Eulerian (ALE) formulation for time-dependent domains, which may include moving boundaries. The Navier-Stokes equations are discretized using a cell-centered finite volume approach on a multi-block grid. The spatial discretization of these equations leads to a set of ordinary differential equations in the temporal domain.

$$\frac{d}{dt}\left(\mathbf{W}_{i,j,k}V_{i,j,k}\right) = -\mathbf{R}_{i,j,k}\left(\mathbf{W}_{i,j,k}\right), \tag{1}$$

where *i,j,k* represent the cell index, **W** and **R** are the vector of conservative flow variables and residual respectively, and $V_{i,j,k}$ is the volume of the cell *i,j,k*. To evaluate the convective fluxes, Osher [15] approximate Riemman solver is used, while the viscous terms are discretized using a second order central difference scheme. The 3rd order MUSCL (Monotone Upstream-centred Schemes for Conservation Laws) approach developed by Leer [16] is used to provide high-order accuracy in space. The HMB3 solver uses the alternative form of the van Albada limiter [17] in regions where large gradients are encountered mainly due to shock waves, avoiding the non-physical spurious oscillations. An implicit dual-time stepping method is employed to perform the temporal integration, where the solution is marching in pseudo-time iterations to achieve a fast convergence. The linearized system of equations is solved using the Generalized Conjugate Gradient method with a Block Incomplete Lower-Upper (BILU) factorization as a pre-conditioner [18]. Multi-block grids allow for the easy balancing of calculation load of high performance parallel computing. In the present work, simulations are performed with the $k-\omega$ SST [19] turbulence model. The HMB3 solver is also equipped with variable mesh methods. It is enabled to handle multi-block, structured grids with sliding planes [9], chimera overset grids [20], and unstructured grids [21]. The chimera method is extensively used in this work.

The Rotating Reference Frame (RRF) method is also implemented in HMB3 for simulations with rotational periodicity, such as rotors in hover or axial flight. The governing flow equations are reformulated and solved in a non-inertial rotating reference frame, which transforms the unsteady problem into steady calculations. This not only reduces significantly the computational cost but also is vital for the adjoint formulation to solve the flow sensitivities. The implementation has been used in previous simulations of ducted fans [22].

The HMB3 solver is also formulated with adjoint formulations to solve the sensitivity equation for gradientbased optimisation. The sensitivity of the cost function $I(\alpha)$ with respect to design variables α can be recast in an adjoint form:

$$\begin{aligned} \left(\frac{\partial \mathbf{R}}{\partial \mathbf{W}}\right)^T \lambda &= -\left(\frac{I}{\partial \mathbf{W}}\right)^T \\ \frac{dI}{d\alpha} &= \frac{\partial I}{\partial \alpha} + \lambda^T \frac{\partial \mathbf{R}}{\partial \alpha}. \end{aligned}, \tag{2}$$

where λ is an adjoint vector correlating the flow and cost equations. Given specified governing flow equations, the scale of this linear system scales only with the number of objective function *I* and is irrelevant to the number of design variables. In this light, the adjoint formulation is especially suitable for optimisation problems involving many design variables.

2.2 Adjoint-based Optimisation Framework

The proposed optimisation framework is described in the flow chart Figure 1. This framework consists of separate tools such as the flow solver, the optimiser, binaries for the mapping between the design space and the geometry, and auxiliary utilities for file I/O and system operations. Each individual tool can be substituted with new methods or implementations, such that the versatility and flexibility of the framework are ensured.

In the current work, objective and constraint functions, as well as, their derivatives to design variables are calculated through the HMB3 Adjoint solver. Once initial HMB3 solutions of the baseline design are checked, the optimiser is initialised and the optimisation loops begin. The optimiser yields new design variables in each iteration, upon input objectives, constraint, and derivatives from previous HMB3 solutions. The new design variables are translated into mesh deformation and are feed to new HMB3 calculations. The optimisation loops stop and output a final set of design variables when pre-established criteria have been met, e.g. derivatives are

approaching zero or upper limits of iterations are met etc. Shell scripts and in-house codes are composed to automate the procedures.

2.3 Parametrisation of Duct Shape and Blade Twist

As has been learned from previous studies, for an axisymmetric ducted propeller, the thrust augmentation mostly comes from the leading edge suction and higher pressures at the diffuser exit. The mid-chord part of

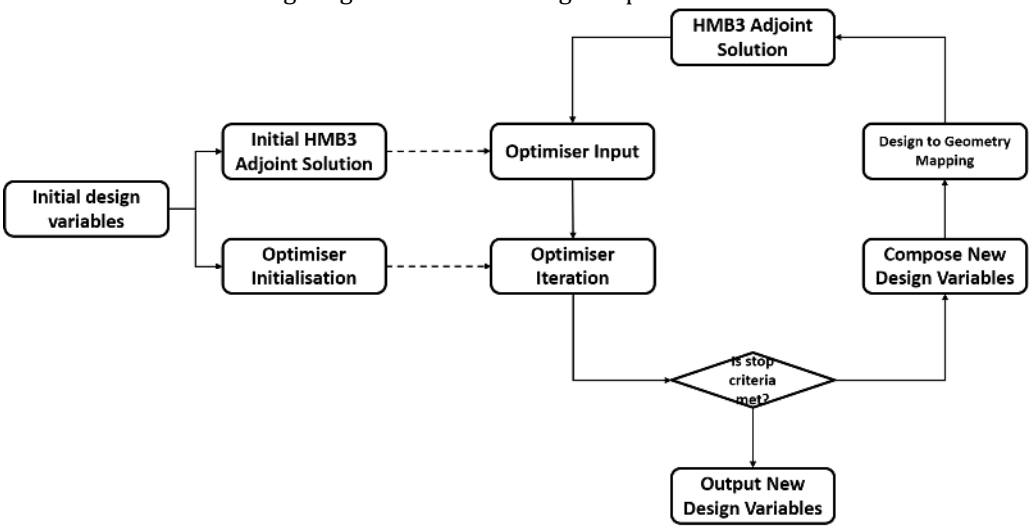

Figure 1: Flow chart of the adjoint-based optimisation.

the duct usually plays a relatively modest role in thrust contribution and is often composed by straight lines in real-world designs. The mid-chord is hence fixed in the current work to exclude varying blade tip gaps and duct thickness. In practice, the duct thickness is also constrained by the structure and the volume. Additionally, the ducted propeller performance is also related to the inlet tip radius, the inlet/outlet expansion ratios, the duct chord length, and the duct camber [4]. In this light, the parametrisation and deformation of duct shapes in this work takes into account the leading-edge and trailing-edge curves, as presented in Figure 2. Nevertheless, the deforming curve region can be extended to include most of the middle chord.

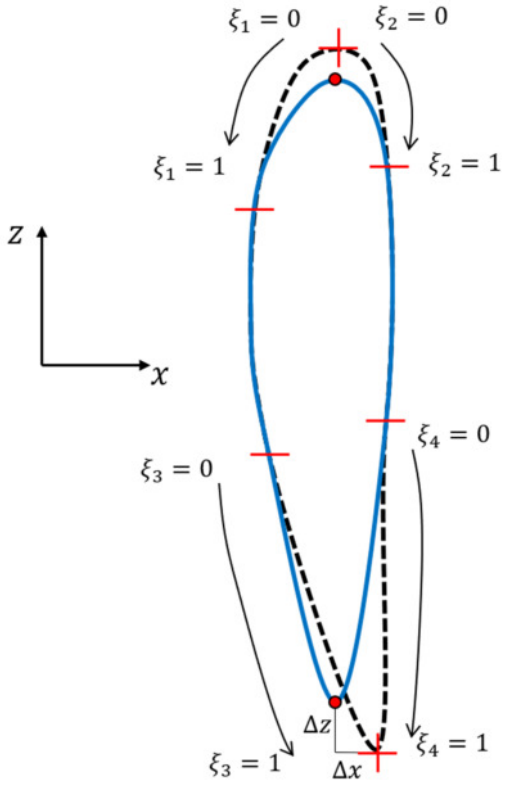

Figure 2: Illustration of duct shape parametrisation.

The proposed parametrisation allows a comprehensive set of variations of duct chord length, camber, inlet lip radius, and inlet/outlet expansion ratios. The design variables are the parameters governing the curve shape, as well as, offsets of the leading/trailing edge points with respect to original positions. The mid-chord region of the duct is fixed. Comparing to other popular parametrisation methods such as Free Form Deformation, the proposed parametrisation approach is strongly physics-based and has excluded a large set of redundant design variables. This duct shape parametrisation problem can be simplified as the parametrisation of 4 curve segments, i.e. the inner leading edge, the outer leading edge, the inner trailing edge, and the outer trailing edge. The curves shapes are locally represented by the classic CST (Class Shape Transformation) method that is often used in aerofoil parametrisation.

Ducted blades typically face higher inflow velocities due to duct induction. It's therefore of interest to investigate blade pitch and twist variations and optimisation while changing the duct shape or axial velocities. The current parametrisation of blade twists is based on polynomial approximations of pitch distributions along the radial direction. The approximation is determined by a set of coefficients, which are therefore considered as the design variables. The pitch distribution is represented by the following equation:

$$\beta(r_0) = \sum_{i=1}^{N} \alpha_i f_i r_0, \tag{3}$$

where $r_0 = r/R$ is the non-dimensional radius. f_i is the basis function (in the current case Bernstein polynomials are used). α_i are coefficients recognised as design variables. N is the number of coefficients. Sample parametrisation of the blade twist used by Grunwald [7] is presented in Figure 3.

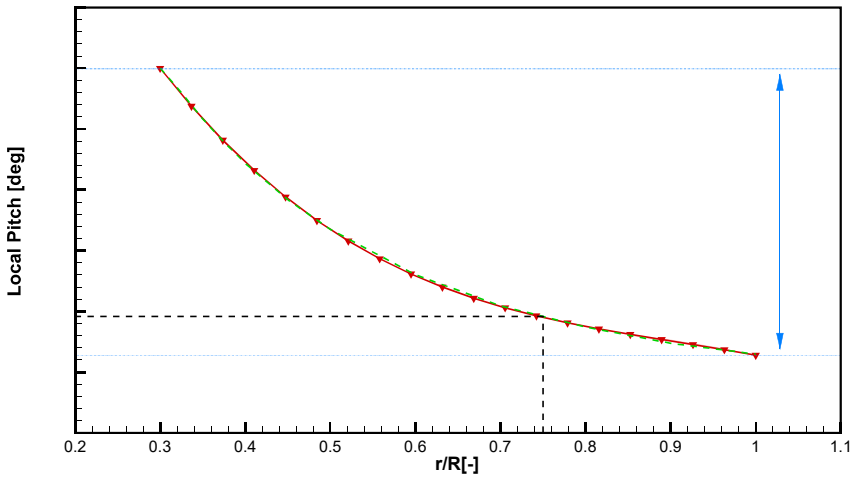

Figure 3: Blade pitch (twist) distributions of the Grunwald blade.

3 Numerical Results

The resolved flow-fields are shown in Figures 4(a) and 4(b). The high-fidelity simulations manage to preserve clearly the tip vortices for 2 to 3 revolutions and 3 to 4 blade radii downstream the rotor disk. Comparisons between experiments and HMB3 simulations, as well as the breakdown of propulsion forces, are listed in Table 1, and good agreement can be noticed between CFD and the test data. Note that all force and moment data are normalized using the far-field dynamic pressure, the duct chord length C_{df}, and the projected duct area S_{df}. Also presented are results for the open propeller configuration at the same pitch and RPM from HMB3. At this advance ratio($\mu = 0.191$) and pitch setting, the ducted and un-ducted configurations produce similar amounts of total thrust, but the ducted propeller requires about 10% less torque and is hence slightly more efficient.

ERROR: ioerror
OFFENDING COMMAND: image

STACK: